Ultrashort Pulsed Neutron Source

I. Pomerantz, E. McCary, A. R. Meadows, A. Arefiev, A. C. Bernstein, C. Chester, J. Cortez,
M. E. Donovan, G. Dyer, E. W. Gaul, D. Hamilton, D. Kuk, A. C. Lestrade, C. Wang, T.
Ditmire, and B. M. Hegelich

An Ultra-Short Pulsed Neutron Source

Revised 10/1/2014

I. Pomerantz[1], E. McCary[1], A.R. Meadows[1], A. Arefiev[2], A. C. Bernstein[1], C. Chester[1], J. Cortez[1],
M. E. Donovan[1], G. Dyer[1], E. W. Gaul[1], D. Hamilton[1], D. Kuk[1], A. C. Lestrade[1], C. Wang[1], T. Ditmire[1]
and B. M. Hegelich[1]

[1]*Center for High Energy Density Science, C1510, The University of Texas at Austin, Austin, Texas 78712, USA*
[2]*Institute for Fusion Studies, The University of Texas, Austin, Texas 78712, USA*
e-mail address: ipom@physics.utexas.edu

We report on a novel compact laser-driven neutron source with unprecedented short pulse duration (<50 ps) and high peak flux ($>10^{18}$ neutrons/cm^2/s), an order of magnitude higher than any existing source. In our experiments, high-energy electron jets are generated from thin (< 3 µm) plastic targets irradiated by a petawatt laser. These intense electron beams are employed to generate neutrons from a metal converter. Our method opens venues for enhancing neutron radiography contrast and for creating astrophysical conditions of heavy element synthesis in the laboratory.

PACS: 29.25.Dz, 52.38.Kd, 52.59.-f, 26.30.-k

Intense neutron generators serve an important role in many research fields, including engineering material science [1], life sciences [2], and condensed matter physics [3]. Until recently the experimental access to a high neutron flux was exclusive to reactor and accelerator-based facilities. For the past few years, the availability of tabletop particle sources based on high intensity lasers has enabled the realization of high flux neutron generators at university-scale laboratories [4,5].

Experimental efforts to optimize laser-based neutron generators have been reported for over four decades [6-9]. Two experiments in the past year [4,10,11] reported laser-generated neutron yields as high as 10^{10} n/sr per laser shot. Their scheme is based on high-energy hydrogen ions emitted from laser-irradiated targets. A piece of beryllium, few cm thick, placed downstream to the target is used to convert the ions into neutrons. An important feature of this method is that the yields and the forward directionality of the emitted neutrons increase with higher ion energies. Therefore, these experiments focused on energy and yield optimization of the emitted ions.

One drawback of this method is low laser-to-ion energy conversion efficiency with typical values at the 1% level [12]. Another is that the resulting neutron pulse is a few 100 ps long, much longer than the sub-ps duration of the laser pulse. The temporal resolution of an experiment conducted using these neutron pulses is no better than that of neutron pulses from conventional ion accelerators.

In this letter, we report on an alternative experimental approach to laser-neutron generation. Our scheme is based on laser-accelerated electrons, not ions. When stopped in a metal converter, these electrons emit high-energy photons (bremsstrahlung gamma rays) that induce nuclear reactions in the converter and release energetic neutrons. The cross sections for these reactions peak for photon energies in the range of 10 – 25 MeV [13,14]. To date, efforts in the laser acceleration of electrons have been focused on reaching the highest possible electron energies, e.g. 2.5 GeV for the laser system used in our experiment [12,15,16]. No effort has been expended on optimizing a laser source of lower energy electrons for neutron production.

We performed our experiment on the Texas Petawatt laser facility at the University of Texas at Austin [17]. The setup is depicted in Fig. 1. Ultra-short laser pulses of 150 fs (FWHM), with 90 J of energy on-target and a wavelength of 1057 nm were focused to a ~10 µm diameter spot on thin
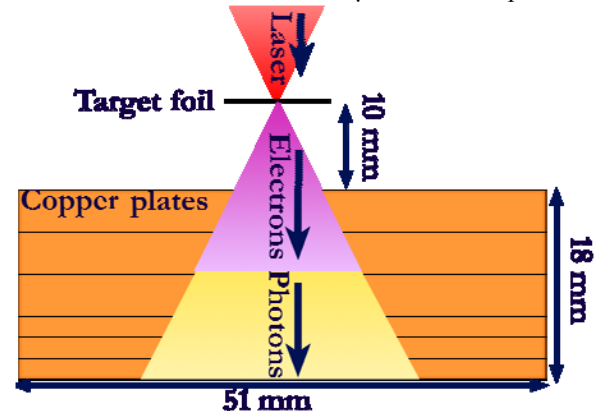

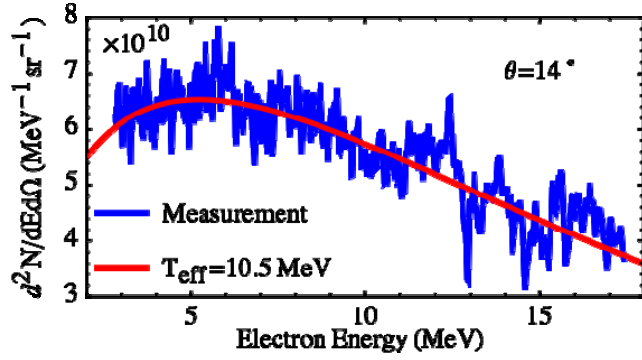FIG. 1 (Color Online). Depiction of the experimental setup. The targets are 0.02 – 3 µm thick plastic foils.

FIG. 2 (Color Online). Electron spectrum measured at a $\theta=14°$ angle with respect to the laser normal. The measurement was performed with the Cu converter removed.
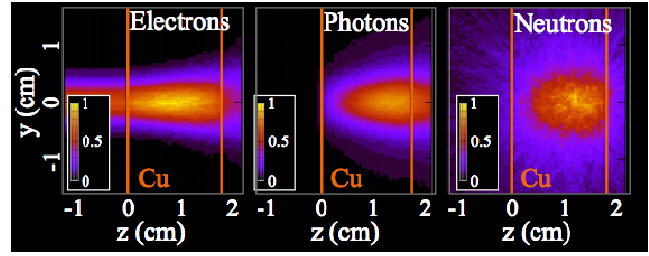

FIG. 3. (Color Online). Simulated particle fluence. The accumulated fluence of electrons (left), photons (center) and neutrons (right) projected on the y-z plane is shown. The edges of the Cu stack are indicated in orange.

$(0.02 - 3 \ \mu m)$ plastic targets. Energy deposited on the target from low-level laser light arriving ~100 ns before the main laser pulse turns the target into an expanding plasma plume [18-20]. Reacting with the plasma plume, the laser pulse creates jets of relativistic electrons that propagate along the laser direction.

The measured energy spectrum of the electrons at a forward angle $(\theta=14°)$ is presented in Fig. 2. These data were taken using a permanent magnet spectrometer positioned 61 cm downstream of the target. A detailed description of this spectrometer is presented in the supplementary note [21]. A fit to a Maxwellian distribution (red curve) yields an effective temperature of 10.5 ± 0.1 MeV, suitable for generating bremsstrahlung radiation within the optimal energy range.

A stack of 9 Cu plates (natural abundance, 69% ^{63}Cu and 31% ^{65}Cu), with a total thickness of 1.8 cm was placed 10 mm downstream of the target. The particle dynamics were studied with the FLUKA particle transport Monte Carlo package [22], the results of which are presented in Fig. 3. In these simulations, a Maxwellian energy distribution with an electron temperature of 15 MeV was assumed [23]. While decelerating in the front layers of the Cu (Fig. 3, left), the electrons generate a high-energy photon beam that propagates deeper into the stack (Fig. 3, center). These photons in turn eject neutrons from Cu nuclei (Fig. 3, right) via the ^{65}Cu$(\gamma,n)^{64}$Cu and ^{63}Cu$(\gamma,n)^{62}$Cu reactions.

The residual radioactive isotopes, ^{64}Cu and ^{62}Cu as well as isotopes produced by competing mechanisms may be individually identified in the Cu plates from half-life decay measurements taken using a Geiger counter. A detailed account of the possible nuclear reactions and their relative contribution to the data presented in this paper is specified in the supplementary note [21].

The induced nuclear activation in the Cu plates was determined and recorded [13] following each shot by placing the Cu plates on an electron-sensitive Fuji MS Imaging Plate (IP) [24]. Exposure times comparable to the decay half-lives of the isotopes of interest were chosen: from t=10 min to t=30 min following the shot. The IP was then scanned using Fujifilm FLA-7000 scanner with 100 μm X 100 μm pixel size.

The activation of the first seven Cu plates in the stack is presented in Fig. 4(a) for shots taken with different target thicknesses. The data shows a clear difference in the particle emission profile between thick (over a few microns) and thin targets. For the targets thicker than a few microns, the target remained intact and overdense (opaque to the laser light) for the duration of both the preliminary pulse and the main laser pulse. In a process known as target-normal sheath acceleration (TNSA), light ion contaminants were accelerated from the back of the solid targets [12,16]. These ions impinged on the Cu and were stopped in the front plate [17,25], as shown in the resulting activation signal. The ion energy distribution was measured using magnetic spectrometers (see supplementary note [21] for details) and found to reach 25 MeV for protons [26,27]. Half-life measurement of the activation signal for these plates verified that the resulting nuclei (^{63}Zn, $\tau_{1/2} = 38$ min) were indeed the product of protons interacting with ^{63}Cu nuclei.

For target thickness of 1 μm and thinner in Fig 4(a), a completely different penetration profile is identified by the activation images. A highly collimated beam-like signal appears throughout the full bulk of the Cu stack. The source of the activation was identified to be the decay of ^{62}Cu ($\tau_{1/2}= 9.7$ min) generated by the ^{63}Cu$(\gamma,n)^{62}$Cu reaction.
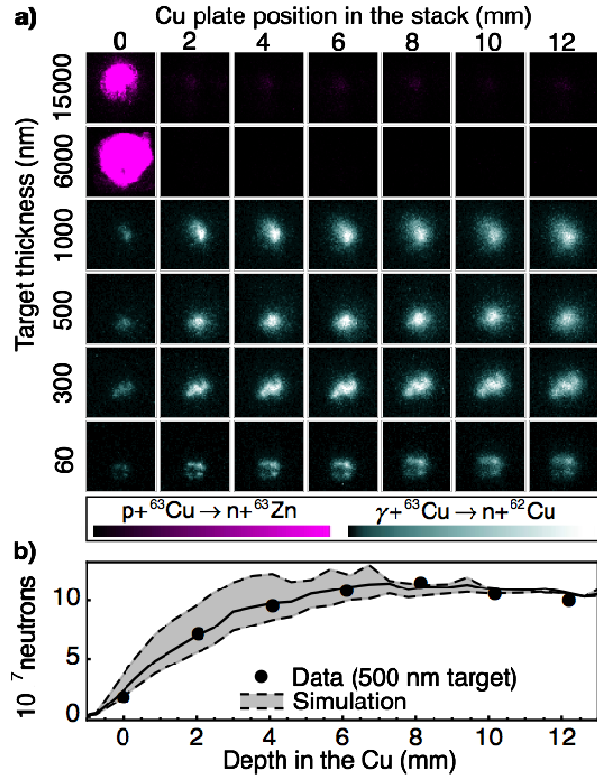
FIG. 4 (Color Online). Autography of the Cu plates. (a) The autographs are images of the activation level in each plate. Each autograph corresponds to an area of 5.1 cm X 5.1 cm. The autographs of the first 7 plates in the stack are shown in each row. (b) The inferred number of neutrons emitted from each plate by the $^{63}Cu(\gamma,n)^{62}Cu$ reaction.

In the context of this work, the difference between the photo-neutron production cross sections off ^{63}Cu and ^{65}Cu is negligible [28], and the measured activation signal accounts for about 60% of the total number of generated neutrons (the relative natural abundance of ^{63}Cu). The $^{65}Cu(\gamma,n)^{64}Cu$ reaction channel accounts for the majority of the rest of generated photo-neutrons, however with the half-life of ^{64}Cu being much longer ($\tau_{1/2}$=12.7 hr), this channel's contribution to the activation signal is smaller than 1.8% [21].

The spatial features of the electron jet are evident from the activation signal. For targets thinner than 300 nm, the jet appears to have filamented and broken up into multiple lobes, while for 500-1000 nm the jet appears to have been a single beam. This remarkable result is consistent with a 15 year old prediction [29-31] obtained using a 3D particle-in-cell simulation of a high intensity laser pulse interacting with underdense (transparent to the laser light) plasma. This simulation shows that the incident beam first propagates through an unstable filamentary stage whereupon the induced 1 kT magnetic fields in the plasma pinch the

electron jets into a single beam. We conclude that the lobes are reminiscent of these filaments, possibly due to a more limited extent of the plasma originating from these thinner targets such that the electron jets emerge before the collapse stage.

The total activity of each Cu plate was calibrated by placing a ^{22}Na beta emitter with activity of 2.3 kBq on the IP for a period of 20 min. This allowed for the total number of neutrons produced by the $^{63}Cu(\gamma,n)^{62}Cu$ reaction in each plate to be calculated with methods described in reference [13]. The number of neutrons is plotted (black circles) in Fig. 4(b) as a function of the plate position in the stack, for a shot on a 500 nm thick target. A 35% uncertainty is associated with the overall normalization of these data, resulting from the fast fading time of the IP [32], however the point-to-point uncertainty is smaller than 5%. Also shown in the figure is the simulated number of neutrons as a function of penetration depth (black line). An uncertainty band (dashed line) determined by simulations assuming electron temperatures of 10 MeV and 20 MeV is presented to demonstrate the sensitivity of the simulation results to the assumed electron temperature of 15 MeV.

The neutrons produced by the $^{63}Cu(\gamma,n)^{62}Cu$ reaction, whose number we determined by nuclear activation-based imaging account for ~60% of the total number of photo-neutrons produced [28]. Therefore, we can infer the total number of neutrons to be $(1.2\pm0.4)\times10^{9}$ for the shot presented in Fig 4(b) (note that only the first 7 plates out of 9 are shown).

In addition, we directly measured neutrons using eight BTI Bubble dosimeters [27,33] positioned outside the experimental chamber at a distance of 80 cm from the interaction point. These were arranged at positions 0º, 30º, 45º, 60º, 90º, 135º, 180º and 335º with respect to the incoming laser direction. The sensitivity of the dosimeters has been studied and found to be quite flat over the range of measured neutron energies [10]. A value of $(3\pm1)\times10^{-5}$ bubbles/neutron/cm^2 was used in the analysis. The manufacturer specified individual efficiency values in the range of 9.1-26.0 bubbles/mrem for each of the dosimeters. We confirmed these sensitivity values within statistical uncertainty by irradiating the dosimeters with 1 mrem of neutrons using a ^{252}Cf source of known activity.

The angular distribution of the neutrons was found to be isotropic within the statistical uncertainty in all shots, as predicted by the simulation. The total number of neutrons measured for different target thicknesses are shown on Fig. 5(a), with their corresponding statistical uncertainties. These values were corrected for the 79% transmission of neutrons passing through the 9 mm thick steel walls of the chamber, as determined from the FLUKA simulation results. An optimum target thickness of 500 nm yielded
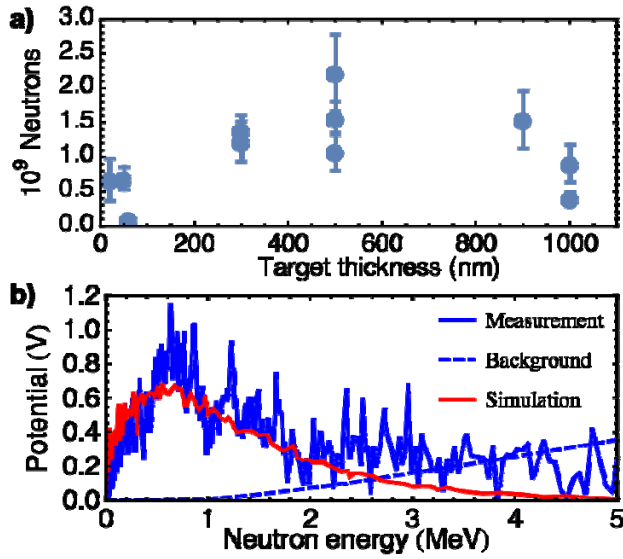
FIG. 5 (Color Online). (a) Target thickness dependence of the total number of neutrons generated per laser shot. Values are interpolated from the neutron dose measured using the Bubble dosimeters. (b) Neutron energy spectrum, measured using Time-Of-Flight technique. The signal is the recorded photomultiplier voltage.

over 10^9 neutrons per shot, in agreement with the total neutron numbers inferred from the activation signal (described above).

The neutron spectral distribution was measured using a neutron time-of-flight (nTOF) detector positioned 360 cm away from the target in the incoming laser direction. The detector is an EJ-232Q plastic scintillator coupled to a fast photomultiplier. A fast digital oscilloscope was used to record the photomultiplier signal. The detector was placed in a lead cave with wall thickness of 40 cm to attenuate the signal of gamma radiation. A small prompt signal from the laser driven gammas arrived ~100 ns prior to the neutrons, which served as a reference for determining the neutron time of flight. The neutron spectrum from a 500 nm thick target is presented in Fig 5b. The background signal from the prompt gamma-rays (dashed blue line) was determined using the method described in [34]. The spectrum matches the expected neutron evaporation spectrum of photo-nuclear reactions in this energy range [35]. The spectrum is in agreement with the FLUKA [22] simulation results (red line) which were absolutely normalized to the data.

A total number in excess of 10^{12} hot electrons in the jet may be inferred from the measured electron spectrum at small forward angle (Fig 2) and the measured divergence of the jet (Fig 4a). This corresponds to a total energy of ~9 J, i.e. ~10% conversion efficiency of laser energy to hot electrons.
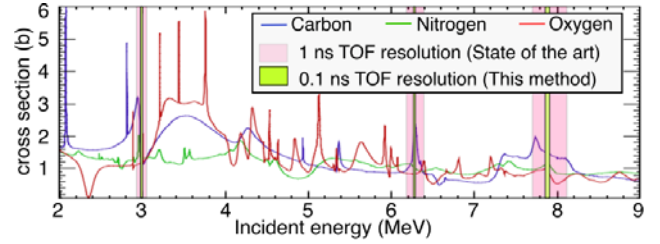

FIG. 6 (Color Online). The total absorption cross-sections for neutrons in carbon (blue), nitrogen (green) and oxygen (red) are shown. The TOF energy resolution for a flight distance of 3.5 m is shown for three example energy values, for the case of 1 ns (pink) and 100 ps (bright green).

With the method reported here, neutrons are generated by photons induced by relativistic *electrons* traversing the converter material at nearly the speed of light. The duration of the electron emission and the target-to-converter temporal dispersion of relativistic electrons are both shorter than a ps. The neutron pulse duration is determined to be less than 50 ps, considering the traverse time of 10 MeV electrons (the threshold for the photo-neutron reaction) in the 1.8 cm long Cu stack. This pulse duration corresponds to a peak neutron flux of 1.1×10^{18} n/cm^2/s, which is emitted isotropically into 4π sr.

This peak neutron flux may be compared with the laser-ion driven method (6×10^{17} n/cm^2/s) [4] as well as with non-laser driven generators like spallation sources (10^{17} n/cm^2/s) [36] and fission reactors (10^{15} n/cm^2/s) [37]. Another laser driven neutron source of interest is the implosion of fusion capsules at the National Ignition Facility. Once reaching "ignition," the neutron flux in the interaction point is expected to exceed 10^{34} n/cm^2/s of DT fusion neutrons [38].

The neutron generator demonstrated here could be ideal for Fast Neutron Resonance Radiography (FNRR) [39]. FNRR takes advantage of the unique neutron absorption spectra of different elements and is used in various research, industry and security applications to study two-phase flow [40] and contraband detection of explosives [41], narcotics [42], and special nuclear materials [43]. In FNRR, neutrons from a pulsed source of a broad energy range are transmitted through the imaged object. Multiple radiographs are taken downstream at several time intervals each corresponding to a different neutron energy bin. The different energy bins can then be correlated to specific absorption energy resonances to yield radiographs of multiple material densities in the sample.

To illustrate the benefit of the short neutron pulse durations achievable with our scheme, the absorption spectra for carbon, nitrogen and oxygen taken from Ref. [44] are plotted in Fig. 6. The sharp absorption resonances

in the few-MeV identify specific elements. The vertical bands on the figure indicate the uncertainty in resolving these resonances for a few example energies using a state-of-the-art 1 ns temporal resolution [39] (pink bands) vs. the 100 ps resolution (green bands) achievable with our scheme. Typical exposure values of FNRR are of 10^8 n/cm^2 [45]. Achieving this exposure will require optimization of our method on laser systems with higher repetition rate.

How heavy elements are created is one of the greatest unanswered questions of modern physics [46]. About half of the elements heavier than Fe and all elements heavier than Bi are produced in nature via the rapid neutron-capture process (r-process). The classic interpretation for the production site of these elements to be at core-collapse supernova explosions [47,48] has recently become a subject of debate with neutron star mergers being the new candidates [49]. In the r-process, heavy isotopes absorb neutrons to become heavier still. The key requirement here is an extremely high flux of neutrons to allow successive neutron absorption in a rate faster than the isotope's decay lifetime. The neutron flux at core-collapse supernova is estimated to be 10^{22} n/cm^2/s [47]. We project that employing our method using a higher Z-number converter like tungsten at laser facilities coming online in the near future [50], will yield a neutron flux in excess of 10^{20} n/cm^2/s. This may enable for the first time the realization of r-process nucleosynthesis conditions in the laboratory.

The experiments reported here were conducted on a laser system capable of delivering one shot per hour. For many applications, including r-process studies and FNRR, the total number of neutrons as well as the instantaneous flux is important. The scalability of our method should be investigated on existing [51] and future [52] laser facilities which are capable of delivering petawatt laser pulses on a high repetition rate.

[1]   W. Reimers, A. R. Pyzalla, A. Schreyer, and H. Clemens, Wiley-VCH Verlag GmbH **42**, ll (2008).

[2]   G. Zaccai, Science **288**, 1604 (2000).

[3]   J. Ma, O. Delaire, A. F. May, C. E. Carlton, M. A. McGuire, L. H. VanBebber, D. L. Abernathy, G. Ehlers, T. Hong, A. Huq, W. Tian, V. M. Keppens, Y. Shao-Horn, and B. C. Sales, Nature Nanotechnology **8**, 445 (2013).

[4]   M. Roth, D. Jung, K. Falk, N. Guler, O. Deppert, M. Devlin, A. Favalli, J. Fernández, D. Gautier, M. Geissel, R. Haight, C. E. Hamilton, B. M. Hegelich, R. P. Johnson, F. Merrill, G. Schaumann, K. Schoenberg, M. Schollmeier, T. Shimada, T. Taddeucci, J. L. Tybo, F. Wagner, S. A. Wender, C. H. Wilde, and G. A. Wurden, Phys. Rev. Lett. **110**, 044802 (2013).

[5]   C. Zulick, F. Dollar, V. Chvykov, J. Davis, G. Kalinchenko, A. Maksimchuk, G. M. Petrov, A. Raymond, A. G. R. Thomas, L. Willingale, V. Yanovsky, and K. Krushelnick, Appl. Phys. Lett. **102**, 124101 (2013).

[6]   G. H. McCall, F. Young, A. W. Ehler, J. F. Kephart, and R. P. Godwin, Phys. Rev. Lett. **30**, 1116 (1973).

[7]   P. A. Norreys, A. P. Fews, F. N. Beg, A. R. Bell, A. E. Dangor, P. Lee, M. B. Nelson, H. Schmidt, M. Tatarakis, and M. D. Cable, Plasma Phys. Control. Fusion **40**, 175 (1998).

[8]   K. L. Lancaster, S. Karsch, H. Habara, F. N. Beg, E. L. Clark, R. Freeman, M. H. Key, J. A. King, R. Kodama, K. Krushelnick, K. W. D. Ledingham, P. McKenna, C. D. Murphy, P. A. Norreys, R. Stephens, C. S. O. eckl, Y. Toyama, M. S. Wei, and M. Zepf, Phys. Plasmas **11**, 3404 (2004).

[9]   D. P. Higginson, J. M. McNaney, D. C. Swift, T. Bartal, D. S. Hey, R. Kodama, S. Le Pape, A. MacKinnon, D. Mariscal, H. Nakamura, N. Nakanii, K. A. Tanaka, and F. N. Beg, Phys. Plasmas **17**, 100701 (2010).

[10]   D. Jung, K. Falk, N. Guler, O. Deppert, M. Devlin, A. Favalli, J. C. Fernández, D. C. Gautier, M. Geissel, and R. Haight, Phys. Plasmas **20**, 056706 (2013).

[11]   I. Pomerantz, J. Blakeney, G. Dyer, L. Fuller, E. Gaul, D. Gautier, D. Jung, A. R. Meadows, R. Shah, C. Wang, J. C. Fernández, T. Ditmire, and M. Hegelich, in (Optical Society of America, 2013), p. QTh3A.4.

[12]   B. M. Hegelich, B. J. Albright, J. Cobble, K. Flippo, S. Letzring, M. Paffett, H. Ruhl, J. Schreiber, R. K. Schulze, and J. C. Fernández, Nature **439**, 441 (2006).

[13]   M. M. Günther, A. Britz, R. J. Clarke, K. Harres, G. Hoffmeister, F. Nürberg, A. Otten, A. Pelka, M. Roth, and K. Vogt, Rev. Sci. Instrum. **84**, 073305 (2013).

[14]   B. L. Berman and S. Fultz, Reviews of Modern Physics **47**, 713 (1975).

[15] X. Wang, R. Zgadzaj, N. Fazel, Z. Li, S. A. Yi, X. Zhang, W. Henderson, Y. Y. Chang, R. Korzekwa, H. E. Tsai, C. H. Pai, H. Quevedo, G. Dyer, E. Gaul, M. Martinez, A. C. Bernstein, T. Borger, M. Spinks, M. Donovan, V. Khudik, G. Shvets, T. Ditmire, and M. C. Downer, Nat Comms **4**, (2013).

[16] S. P. Hatchett, C. G. Brown, T. E. Cowan, E. A. Henry, J. S. Johnson, M. H. Key, J. A. Koch, A. B. Langdon, B. F. Lasinski, and R. W. Lee, Phys. Plasmas **7**, 2076 (2000).

[17] M. Martinez, E. Gaul, T. Ditmire, S. Douglas, D. Gorski, W. Henderson, J. Blakeney, D. Hammond, M. Gerity, J. Caird, A. Erlandson, I. Iovanovic, C. Ebbers, and B. Molander, in *Boulder Damage Symposium XXXVII: Annual Symposium on Optical Materials for High Power Lasers*, edited by G. J. Exarhos, A. H. Guenther, K. L. Lewis, D. Ristau, M. J. Soileau, and C. J. Stolz (SPIE, 2005), pp. 59911N–59911N–9.

[18] D. Giulietti, M. Galimberti, A. Giulietti, L. Gizzi, M. Borghesi, P. Balcou, A. Rousse, and J. Rousseau, Phys. Rev. E **64**, 015402 (2001).

[19] D. Giulietti, M. Galimberti, A. Giulietti, L. A. Gizzi, R. Numico, P. Tomassini, M. Borghesi, V. Malka, S. Fritzler, M. Pittman, K. Ta Phouc, and A. Pukhov, Phys. Plasmas **9**, 3655 (2002).

[20] T. E. Cowan, M. Roth, J. Johnson, C. Brown, M. Christl, W. Fountain, S. Hatchett, E. A. Henry, A. W. Hunt, and M. H. Key, Nuclear Instruments and Methods in Physics Research Section a: Accelerators, Spectrometers, Detectors and Associated Equipment **455**, 130 (2000).

[21] See Supplemental Material at [*URL will be inserted by publisher*].

[22] G. Battistoni, S. Muraro, P. R. Sala, F. Cerutti, A. Ferrari, others, AIP Conf.Proc. **896**, 31 (2007).

[23] The electron spectrum in Fig. 2 was measured on a different run period, in which a reduced laser energy of 70 J was available. An electron temperature of 15 MeV was chosen in the simulation as a better representations of the rest of the dataset.

[24] http://www.fujifilm.com/products/.

[25] J. F. Ziegler, M. D. Ziegler, and J. P. Biersack, Nuclear Instruments and Methods in Physics Research Section B: Beam Interactions with Materials and Atoms **268**, 1818 (2010).

[26] B. M. Hegelich, I. Pomerantz, L. Yin, H. C. Wu, D. Jung, B. J. Albright, D. C. Gautier, S. Letzring, S. Palaniyappan, R. Shah, K. Allinger, R. Hörlein, J. Schreiber, D. Habs, J. Blakeney, G. Dyer, L. Fuller, E. Gaul, E. McCary, A. R. Meadows, C. Wang, T. Ditmire, and J. C. Fernández, New J. Phys. **15**, 085015 (2013).

[27] I. Pomerantz, J. Blakeney, G. Dyer, L. Fuller, E.

Gaul, D. C. Gautier, D. Jung, A. R. Meadows, R. Shah, C. Wang, J. C. Fernández, T. Ditmire, and B. M. Hegelich, in *SPIE Optics + Optoelectronics*, edited by E. Esarey, C. B. Schroeder, W. P. Leemans, K. W. D. Ledingham, and D. A. Jaroszynski (SPIE, 2013), pp. 87791L–87791L–6.

[28] S. Fultz, R. Bramblett, J. Caldwell, and R. Harvey, Phys. Rev. **133**, B1149 (1964).

[29] G. Battistoni, F. Cerutti, A. Fasso, A. Ferrari, S. Muraro, J. Ranft, S. Roesler, and P. R. Sala, in (2007), p. 31.

[30] M. Honda, J. Meyer-ter-Vehn, and A. Pukhov, Phys. Plasmas **7**, 1302 (2000).

[31] A. Pukhov and J. Meyer-ter-Vehn, Phys. Rev. Lett. **76**, 3975 (1996).

[32] K. A. Tanaka, T. Yabuuchi, T. Sato, R. Kodama, Y. Kitagawa, T. Takahashi, T. Ikeda, Y. Honda, and S. Okuda, Rev. Sci. Instrum. **76**, 013507 (2004).

[33] Bubble technology industries http://bubbletech.ca/.

[34] D. Jung, R. Hörlein, D. C. Gautier, S. Letzring, D. Kiefer, K. Allinger, B. J. Albright, R. Shah, S. Palaniyappan, L. Yin, J. C. Fernández, D. Habs, and B. M. Hegelich, Rev. Sci. Instrum. **82**, 043301 (2011).

[35] J. M. Blatt, *Theoretical Nuclear Physics* (Courier Dover Publications, 1991).

[36] S. C. Vogel and J. S. Carpenter, Jom **64**, 104 (2012).

[37] M. A. Garland, S. Mirzadeh, C. W. Alexander, G. J. Hirtz, R. W. Hobbs, G. A. Pertmer, and F. F. Knapp Jr, Applied Radiation and Isotopes **59**, 63 (2003).

[38] E. I. Moses, **112**, 012003 (2008).

[39] D. Vartsky, I. Mor, M. B. Goldberg, D. Bar, G. Feldman, V. Dangendorf, K. Tittelmeier, M. Weierganz, B. Bromberger, and A. Breskin, Nuclear Instruments and Methods in Physics Research Section a: Accelerators, Spectrometers, Detectors and Associated Equipment **A623**, 603 (2010).

[40] N. Takenaka, H. Asano, T. Fujii, M. Mizubata, and K. Yoshii, Nuclear Instruments and Methods in Physics Research Section a: Accelerators, Spectrometers, Detectors and Associated Equipment **424**, 73 (1999).

[41] J. C. Overley, M. S. Chmelik, R. J. Rasmussen, R. Schofield, and H. W. Lefevre, Nuclear Instruments and Methods in Physics Research Section B: Beam Interactions with Materials and Atoms **99**, 728 (1995).

[42] C. L. Fink, B. J. Micklich, T. J. Yule, P. Humm, L. Sagalovsky, and M. M. Martin, Nuclear Instruments and Methods in Physics Research

Section B: Beam Interactions with Materials and Atoms **99**, 748 (1995).

[43]   J. Rynes, J. Bendahan, T. Gozani, R. Loveman, J. Stevenson, and C. Bell, Nuclear Instruments and Methods in Physics Research Section a: Accelerators, Spectrometers, Detectors and Associated Equipment **422**, 895 (1999).

[44]   V. Mclane, *ENDF-102 Data Formats and Procedures for the Evaluation Nuclear Data File ENDF-6.* (2001).

[45]   V. Dangendorf, G. Laczko, C. Kersten, O. Jagutzki, and U. Spillmann, arXiv **nucl-ex**, (2003).

[46]   *Connecting Quarks with the Cosmos: Eleven Science Questions for the New Century* (National Academies Press, 2003).

[47]   M. E. Burbidge, G. R. Burbidge, W. A. Fowler, and F. Hoyle, Rev. Mod. Phys. **29**, 547 (1957).

[48]   G. Wallerstein, I. Iben, P. Parker, A. Boesgaard, G. Hale, A. Champagne, C. Barnes, F. Käppeler, V. Smith, R. Hoffman, F. Timmes, C. Sneden, R. Boyd, B. Meyer, and D. Lambert, Rev. Mod. Phys. **69**, 995 (1997).

[49]   C. Freiburghaus, S. Rosswog, and F. K. Thielemann, ApJ **525**, L121 (1999).

[50]   G. Mourou and T. Tajima, Optics and Photonics News **22**, 47 (2011).

[51]   W. P. Leemans, J. Daniels, A. Deshmukh, A. J. Gonsalves, A. Magana, H. S. Mao, D. E. Mittelberger, K. Nakamura, J. R. Riley, and D. Syversrud, in *Proceedings of PAC 2013 (JaCoW, 2013), P. THYAA1* (2013).

[52]   G. Mourou, B. Brocklesby, T. Tajima, and J. Limpert, Nature Photonics **7**, 258 (2013).